Analytical Methods

ROYAL SOCIETY OF CHEMISTRY

PAPER

View Article Online
View Journal | View Issue

Cite this: *Anal. Methods*, 2023, **15**, 322

CNN-assisted SERS enables ultra-sensitive and simultaneous detection of Scr and BUN for rapid kidney function assessment

Ping Lu,[a] Dajun Lin,[b] Ning Chen,[a] Luyao Wang,[a] Xuedian Zhang,[c] Hui Chen[a] and Pei Ma*[a]

Kidney disease is highly prevalent and may result in severe clinical outcomes. Serum creatinine (Scr) and blood urea nitrogen (BUN) are the most widely used biomarkers for kidney function assessment, yet when measured alone, the result can be affected by a variety of parameters such as age, gender, protein consumption, *etc.* Measuring Scr and BUN simultaneously can eliminate most of the external influences and greatly improve the assessment of kidney function. In this study, a real-time kidney function assessment system based on dual biomarker detection was proposed. Scr and BUN were determined using surface-enhanced Raman scattering (SERS) within the concentration range of 10^{-1} to 10^{-6} M and 0.28 to 100 mg dl^{-1}, respectively. A one-dimensional convolutional neural network (1D-CNN) model was employed to quantitatively analyze the concentration of biomarkers from the SERS spectral measurements. Moreover, we simulated a variety of kidney health conditions with 16 groups of mixed Scr and BUN in serum. The proposed CNN-assisted SERS method was used to quantify both biomarkers and provide diagnostic results. The Au core-Ag shell nanoprobes provided ultra-sensitive SERS detection and the CNN model achieved excellent regression results with an R^2 of 0.9871 in the testing dataset. The system demonstrated a rapid and robust evaluation for the assessment of kidney function, providing a promising idea for medical diagnosis with the help of spectroscopy and deep learning methods.

Received 27th September 2022
Accepted 12th December 2022

DOI: 10.1039/d2ay01573k

rsc.li/methods

1. Introduction

The kidney is primarily used to excrete metabolic waste from the human body and the health condition of the kidney is extremely important in assessing the body's function.[1] Serum creatinine (Scr) is currently the most commonly used renal biomarker in clinics. It is the final metabolite of human muscle, being released into the blood and continuously passing to the kidney for clearance.[2,3] Failure of clearance of creatinine indicates severe dysfunction of the kidney.[4] However, renal function cannot be accurately assessed with the concentration of Scr only because the Scr concentration can be affected by factors such as age, gender, weight, *etc.*[5,6] The increase in muscle mass also results in a substantial increase in Scr.[7] In clinics, the concentration of Scr is usually combined with urine output and other symptoms to diagnose kidney function.[8] Measuring the concentrations of multiple biomarkers simultaneously may be a better solution, because different biomarkers are associated with different mechanisms, giving more robust judgements. For example, Scr can be measured simultaneously with blood urea nitrogen (BUN), the amount of nitrogen contained in urea.[9,10] Healthy kidneys remove urea from the bloodstream and the concentration of BUN rises when the kidney is damaged.[11] The concentration of BUN is less susceptible to age or gender, but it can be affected by high consumption of proteins. Hence, the content level of Scr and BUN together can more accurately reflect kidney health conditions. An effective and convenient method of simultaneously measuring the concentration of Scr and BUN can greatly help the diagnosis of renal function.

Conventional methods are generally not suitable for the simultaneous detection of Scr and BUN. The most commonly used methods for Scr or BUN measurement in clinics and laboratories are Jaffe reaction spectrophotometry,[12–14] high-performance liquid chromatography (HPLC),[15] microfluidic chip,[10,16] enzymatic digestion,[17] liquid chromatography tandem mass spectrometry (LC-MS/MS)[18,19] and so on. Jaffe reaction spectrophotometry only roughly measures the Scr concentration by the degree of redness of the complex obtained by reaction of picric acid with creatinine. LC-MS/MS requires a series of steps such as lysis, elution and so on using large professional equipment to measure the content of Scr or BUN. These

[a]*Key Laboratory of Optical Technology and Instrument for Medicine, Ministry of Education, College of Optical-Electrical and Computer Engineering, University of Shanghai for Science and Technology, Shanghai 200093, China. E-mail: peima@usst.edu.cn*

[b]*Department of Electrical and Computer Engineering, The University of Utah, Salt Lake City, UT 84112, USA*

[c]*Shanghai Institute of Intelligent Science and Technology, Tongji University, Shanghai 200092, China*

methods can be highly sensitive; however, they have drawbacks including high cost, complicated operation, and requiring specialized personnel. More importantly, these methods only measure one compound at one time. These drawbacks have hindered the measurement and analysis of multiple biomarkers simultaneously, making the results less reliable.

In order to provide the ability of simultaneously measuring both Scr and BUN concentrations, a rapid, non-contact and highly sensitive surface-enhanced Raman spectroscopy (SERS) method with a Au@Ag substrate was proposed. SERS was based on localized surface plasmon resonance (LSPR) of metal nanoparticles to greatly enhance the weak Raman signals,[20,21] which contain unique characteristic peaks reflecting the vibrational modes of molecules. SERS of a sample with multiple chemicals would present characteristic peaks of all chemicals, and can therefore be used to identify the content of each chemical.[22,23] Besides the position of characteristic peaks, the intensity of the SERS spectrum is a reflection of chemical concentration, providing the ability of quantification.[24] Therefore, SERS is a very promising technique to simultaneously determine the concentrations of two renal biomarkers Scr and BUN. However, compared to single chemical quantification, in which SERS usually has excellent linear responses, quantification of a mixture of chemicals faces difficulties including nonlinear responses, overlapping characteristics peaks, ignoring peaks with low intensity, *etc.* Traditional methods such as partial least-squares regression (PLSR), support vector regression (SVR), multiple linear regression (MLR), and fully connected neural networks (FNN), lack learning abilities and are unable to precisely identify complex spectra, especially on large-scale data with a low signal-to-noise ratio and subtle differences. Recently, deep learning has shown potential in complex Raman spectral quantitative analysis. Particularly, CNN has convolutional kernel features to extract Raman spectral features, showing remarkable abilities in reducing computational effort and effective quantification of biomarkers.[25] Xu Yan[26] has developed quantitative calibration models using CNN based on Raman spectroscopy for the GH hydrolysis process. Chao Ni[27] has predicted the leaf nitrogen content of Masson pine seedlings using a CNN model based on near-infrared spectroscopy.

In this paper, we proposed a SERS and CNN-based dual-biomarker detection system, which was able to simultaneously quantify spectroscopic data of two renal biomarkers in serum, Scr and BUN (Fig. 1). 16 groups of mixed Scr and BUN with a variety of concentrations were investigated with SERS. The concentration combinations were designed to represent different conditions of kidney function. Gold core-silver shell structure nanoparticles (Au@Ag NPs) were used as SERS substrates, which greatly increase the Raman signals of the biomarkers. To predict the content of Scr and BUN in mixed solutions, each spectrum was converted into a one-dimensional vector as the input of a CNN-based deep learning model[28] (Fig. 1a). The model was equipped with sliding convolutional kernels to automatically extract features of different concentrations of multiple biomarkers. The predicted results were obtained after the passing convolutional layers and fully-connected layers in the network (Fig. 1b). Finally, concentrations of Scr and BUN were predicted and the renal function can

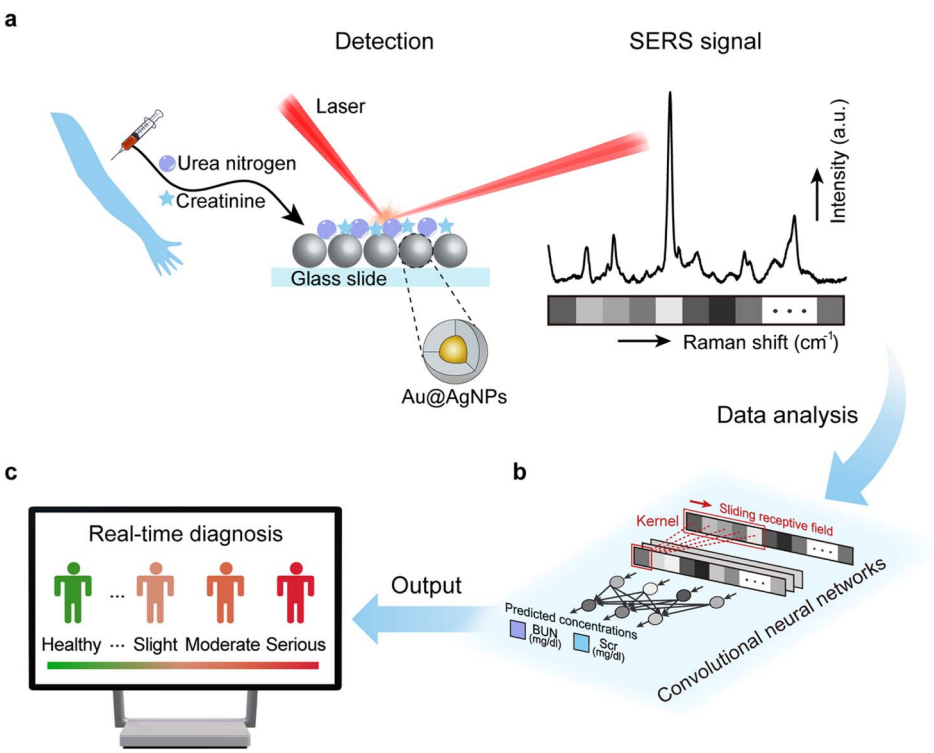

Fig. 1 Schematic illustration of a CNN-based human kidney function assessment system by using SERS. (a) SERS detection of mixed creatinine and urea nitrogen in serum. (b) CNN model for quantitative analysis of SERS spectroscopic data. (c) Real-time diagnosis of kidney function.

be assessed in real-time. A combination of SERS and CNN was demonstrated to be a strong helper in the diagnosis of renal functions. The proposed method also has great potential in a variety of clinical applications that involve multi-biomarker detection.

2. Materials and methods

2.1 Chemicals and reagents

Chloroauric acid tetrahydrate ($HAuCl_4 \cdot 3H_2O$), silver nitrate solution ($AgNO_3$), sodium citrate dihydrate ($C_6H_5Na_3O_7 \cdot 2H_2O \geq 99.0\%$), creatinine ($C_4H_7N_3O$, 99%), and urea standard solution, were purchased from MACKLIN (Shanghai, China). Deionized water with a resistivity of 18.25 MΩ was used to dilute the above reagents for the experiments. Fetal bovine serum was purchased from Hangzhou Four Seasons Green Biological Engineering Co.

2.2 Synthesis of AuNPs and Au@Ag NPs

Au core-Ag shell nanoparticles were synthesized to combine the advantages of Au and Ag. The SERS effect was suggested to be induced by the formation of surface plasmon resonance at the gap of nanoparticles, resulting in hot spots,[29,30] where the signal intensity of the target molecule got significantly enhanced (Fig. 2a). Ag NPs were demonstrated to have ideal SERS enhancement while Au NPs were known for their chemically stability and they are well dispersed with a uniform particle size.[31] Based on that, we prepared Au core-Ag shell nanoparticles.

In this study, Au NPs were obtained by the reduction of $HAuCl_4$ according to the method of FrensG.[32] 250 μL of 1 wt% $HAuCl_4 \cdot 4H_2O$ solution and 250 ml deionized water were added to a clean beaker, stirred, and heated until boiling. Then 2.5 ml of sodium citrate solution (1 wt%) was added. The solution was vigorously stirred and boiled for 15 min before it was cooled down to room temperature. Then the solution was centrifuged at 9500 rpm for 15 min and the supernatant was removed to obtain Au NPs.

To obtain Au@Ag NPs, the concentrated gold nanoparticles were diluted and dispersed in 250 ml of deionized water. Subsequently, it was continuously stirred and heated to 60 °C. When it boils, 6 ml of 1 wt% sodium citrate solution and 2.5 ml of 0.1 M silver nitrate solution[33] were added (Fig. 2b). The color of the mixed solution changed from purple to caramel. Au@Ag NPs were formed and were then cooled down to room temperature for further use. The Au@Ag NPs were characterized using several tools. The UV-absorption spectra of Au NPs and Au@Ag NPs were obtained by using a UV-3600 spectrometer (Shimadzu, Japan) in the wavelength range of 300–800 nm. Transmission electron microscopy (TEM, FEI, Hillsborough, or the United States) images were acquired to observe the shape and distribution of the nanoparticles. Particle size distribution images were measured by using a Zetasizer, (Nano-ZS90, Mohr Wen, UK). The enhancement effect of Au@Ag NPs were compared with that of Au NPs by measuring Rhodamine 6G (R6G) at a concentration of 10^{-4} M.

2.3 Preparation of creatinine and urea nitrogen standards and serum solution

Creatinine powder was added to different volumes of deionized water to obtain creatinine standard solutions of six concentrations (10^{-1} M, 10^{-2} M, 10^{-3} M, 10^{-4} M, 10^{-5} M, and 10^{-6} M, corresponding to 0.0113 mg dl^{-1} to 1131.2 mg dl^{-1}). The urea nitrogen solution was added to different volumes of deionized water to acquire urea nitrogen standard solutions of different

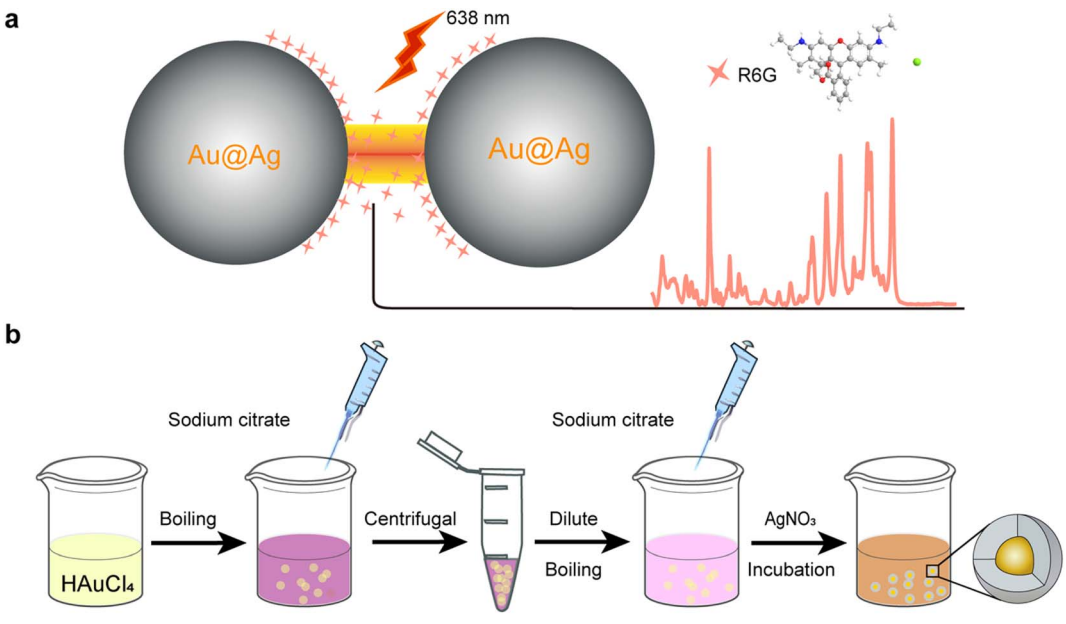

Fig. 2 Fabrication of Au@Ag NPs. (a) 'Hot spots' formed between Au@Ag NPs and sample molecules (R6G). (b) The synthesis process of the Au@Ag NP colloid.

concentrations (100 mg dl^{-1}, 50 mg dl^{-1}, 28 mg dl^{-1}, 2.8 mg dl^{-1}, and 0.28 mg dl^{-1}).

Fetal bovine serum was utilized as a simulated biological environmental fluid. Both urea nitrogen serum samples (BUN) and creatinine serum samples (Scr) were prepared by replacing deionized water with fetal bovine serum, and the rest of the parameters were unchanged when compared to those of the standard solutions. The creatinine and urea nitrogen serum mixed solutions were prepared by mixing the two biomarkers to reach certain concentrations. In this study, we used fetal bovine serum to simulate the serum environment, and utilized rationed biomarkers to simulate different degrees of kidney health. All mixed solutions were prepared in fetal bovine serum to simulate human serum.

In healthy individuals, the concentration range of Scr is 0.5–1.2 mg dl^{-1}, and that of BUN is usually within 5–20 mg dl^{-1}.[10] The concentrations of Scr or BUN can be increased with kidney dysfunction, up to 73.8 mg dl^{-1} (ref. 34) and 120 mg dl^{-1} (ref. 35) and beyond. However, when measured separately, the results can be confusing because parameters such as age, gender, muscle content and protein intake can affect Scr or BUN concentrations. Increases in both biomarkers provide a more definite signal of kidney dysfunction.[36–44]

Here, we prepared 16 groups of mixed solutions to include a wide range of BUN and Scr concentrations, normal to abnormal, as shown in Table 1. The colors were used to differentiate healthy degrees of the kidney. Concentrations of both biomarkers within a normal range were colored in green. Orange shaded areas were displayed to represent possibly healthy or a slightly unhealthy trend of the kidney, with one biomarker exceeding its normal concentration range.

The red shaded area represented severely abnormal renal function, with BUN and Scr concentrations exceeding the healthy range. In the first column (Scr 0.8 mg dl^{-1} and BUN 4–28 mg dl^{-1}), the first three situations were absolutely healthy with both biomarkers being normal while the last one was possibly normal because 28 mg dl^{-1} BUN was likely caused due to high protein consumption.[36] In the second column (Scr 2.1 mg dl^{-1} and BUN 10.5–73.5 mg dl^{-1}), renal dysfunction was present when both biomarkers exceeded their normal range, as shown in the three red cells. Yet the orange cell where Scr is abnormal with BUN being normal may represent a situation of a person with the course of a strenuous prolonged endurance activity.[37] The other two columns can be explained similarly (constant BUN and varying Scr). It can be observed that different health conditions of the kidney exist with the same Scr (BUN) concentrations. And with simultaneous detection of Scr and BUN, a more accurate judgement can be made.

2.4 SERS signal acquisition and pre-processing

All Raman and SERS spectra were acquired with a confocal Raman microscope (XploRA PLUS, HORIBA). We chose a 638 nm laser with 3 mW power which can avoid the fluorescence background, provide good sensitivity and obtain an effective spectrum in 2 s of exposure time. We used Au@Ag NPs as SERS substrates and performed SERS detection on all samples. The spectrum for each single biomarker solution was obtained by averaging 8 independent measurements. The linear relationship between the SERS characteristic peak intensity and concentration of solution was established. A larger R^2 indicates a better linear response between the peak intensity and the concentration. Generally, a large amount of training data should be collected and input into the CNN network. In this study, we experimentally collected SERS spectra from 16 groups of mixed biomarker serum solutions according to Table 1, reflecting a variety of kidney functions from healthy to serious malfunction. In each group, 40 SERS spectra were collected, measured at random locations on the samples. This resulted in a total number of 640 (16 × 40) raw spectra. 80% of the spectral data of each group were randomly chosen as the training dataset, and the remaining 20% were used as the testing dataset. The size of the dataset and the split ratio were determined based on the literature and experience.[45–47] In addition, before entering the CNN network, the SERS spectral data were pre-processed to reduce noise and

Table 1 16 groups of creatinine and urea nitrogen mixed solutions and diagnosis of kidney function[a]

	Ratio	Consistent Scr concentration (mg/dl)				Consistent BUN concentration (mg/dl)			
		BUN	Scr	BUN	Scr	BUN	Scr	BUN	Scr
Concentration (mg/dl)	5:1	4 0.8 [38]		10.5 2.1 [37,39]		15 3 [40]		40 8 [40,41]	
	15:1	12 0.8 [38,42]		31.5 2.1 [41]		15 1 [38,42]		40 2.7 [41]	
	25:1	20 0.8 [38,42]		52.5 2.1 [41]		15 0.6 [38,42]		40 1.6 [39]	
	35:1	28 0.8 [36,40]		73.5 2.1 [41,43,44]		15 0.43 [38,42]		40 1.14 [39]	

[a] The degree of kidney dysfunction related to each concentration combination of Scr and BUN was supported by references [36–44], as labelled in each cell.

remove the baseline in labspec6 (Software kit) for better presentation.

2.5 CNN model for SERS data analysis

The 1D-CNN was proposed to predict the concentrations of mixed Scr and BUN measured with SERS. As illustrated in Fig. 3, the proposed CNN architecture consists of an input layer, 6 hidden layers, 2 fully connected layers and an output layer. Each layer was interconnected, processing information, and extracting features of the SERS spectrum data. First, the data of SERS spectra were flattened into one-dimensional vectors (1 × 957 grayscale matrices) along the SERS shift axis. Then, a 1 × 1 convolution was used to expand the channel number. After that, 5 convolutional layers with a kernel size of 1 × 5, 1 × 5, 1 × 5, 1 × 5 and 1 × 3, respectively, were used. The output feature channel number of each of these convolutional layers became twice that of the previous layer. If the convolutional layer was represented by a weight vector W of length R with stride S, and its input feature size was N, then by the definition of convolution, its output feature size becomes $(N - R)/S + 1$. The ReLU activation function was added after each convolution layer, expressed as $\boldsymbol{a}^{\mathbf{l}} = \mathbf{ReLU}(\boldsymbol{a}^{\mathbf{l-1}} \times \boldsymbol{W}^{\mathbf{l}} + \boldsymbol{b}^{\mathbf{l}})$, where $\boldsymbol{a}^{\mathbf{l}}$ refers to the output of each layer, $\boldsymbol{a}^{\mathbf{l-1}}$ refersto the input, $\boldsymbol{W}^{\mathbf{l}}$ refers to the convolutional filters and $\boldsymbol{b}^{\mathbf{l}}$ is the bias. Afterwards, the feature was fed into 2 fully connected layers before the output. Besides, we applied three MaxPooling layers with a size of 1 × 2 along with the last 3 convolutional layers, performing dimension reduction and smoothing compression. Before entering the fully connected layers, the feature map reached a size of 512 × 3. Finally, a Softmax function was used to map the feature into a probability distribution of multiple nodes, and only the max probability node was activated for the single output. During training, dropout operations with a probability of 0.5 was used in the two fully connected layers to prevent over-fitting in this model.

The performance of the model was evaluated by using R^2, shown in eqn (1).

$$R^2 = 1 - \frac{\sum_{n=1}^{N}(\hat{y}_n - y_n)^2}{\sum_{n=1}^{N}(y_n - \bar{y})^2} \quad (1)$$

where y_n and $\hat{y}_n$ are the ground truth and predicted value. $\bar{y}$ is the mean value, and N is the total number of training or testing sets.

The measured intensity of SERS data will linearly increase based on the integration time of the spectrometer and fluctuate with background noise in each test. Assuming that the trained model memorizes the noise and irrelevant information from sample data, the model will become overfitted and cannot generalize well to new date. As such, L2 Regularization is necessary in the training to prevent over-fitting.[48] The sum of the squared magnitude of weights in the 1D-CNN model was penalized and added to the loss function, which could be expressed as:

$$\mathrm{LOSS} = \frac{1}{N}\sum_{n=1}^{N}[y_n - \hat{y}_n]^2 + \lambda\sum \|w\|_2^2 \quad (2)$$

where λ was chosen as 0.01 and weights close to zero have little effect on model complexity.

The root mean square error (RMSE) is an indicator for error analysis. The RMSE can be calculated using eqn (3).

$$\mathrm{RMSE} = \sqrt{\frac{1}{n}\sum_{i=1}^{n}(\mathrm{Predicted}_i - \mathrm{Actual}_i)^2} \quad (3)$$

where n is the number of samples. $\mathbf{Predicted}_i$ and $\mathbf{Actual}_i$ is the predicted actual concentration in the model.

3. Results and discussion

3.1 Characterization of Au@Ag NPs

The UV-absorption spectra of Au NPs and Au@Ag NPs, measured by using a UV-Vis spectrophotometer, are shown in Fig. 4. Au NPs presented a strong absorption peak at 520 nm, which coincides with the surface plasmon resonance of gold (Fig. 4a). For Au@Ag NPs, a shoulder peak appeared at approximately 420 nm, showing the transverse plasmonic absorption nature of silver.[49]

Au NPs and Au@Ag NPs were further characterized by TEM (Fig. 4b and c). The particle sizes of Au NPs and Au@Ag NPs were approximately 28 nm and 45 nm respectively, with good uniformity. It can be observed in Fig. 4c that a gold core was at the center of each particle, wrapped with a shell outside, which was dispersed and uniform in shape.

The enhancement effect of Au NPs and Au@Ag NPs was compared by SERS assays performed on Rhodamine 6G (R6G) at a concentration of 10^{-4} M. The signal intensity of Au@Ag NPs was approximately twice the signal intensity of Au NPs at 1650 cm^{-1} (Fig. 4d).

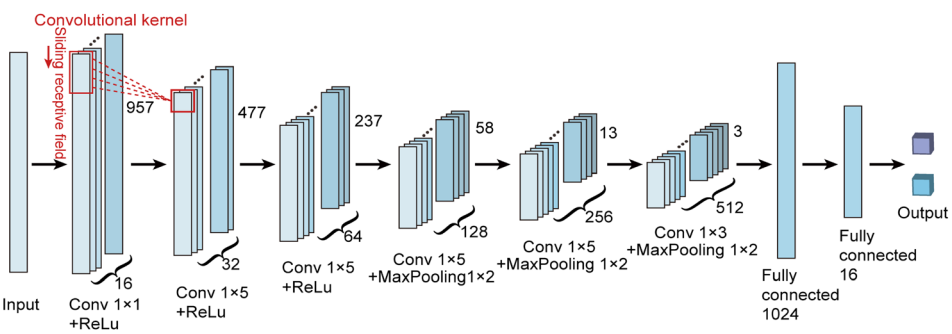

Fig. 3 Architecture of the proposed 1-CNN model.

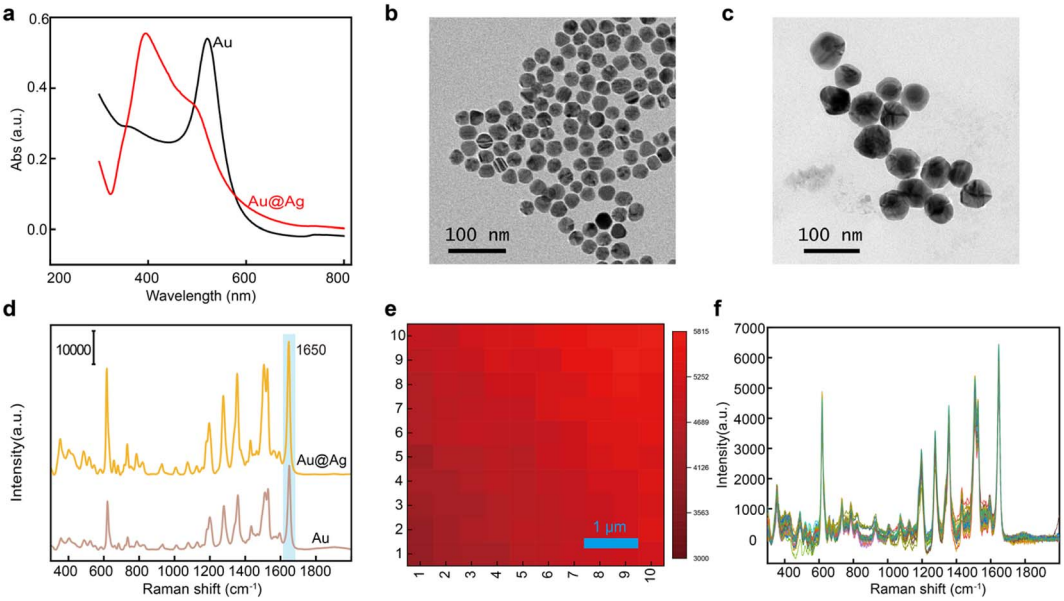

Fig. 4 Characterization studies of Au NPs and Au@Ag NPs. (a) UV-Vis absorption spectra of Au NPs (black line) and Au@Ag NPs (red line). (b) and (c) TEM images of Au NPs and Au@Ag NPs, respectively. (d) Comparison of enhancement effect based on Au NPs and Au@Ag NPs. (e) The SERS mapping image at 1650 cm^{-1} of R6G. (f) SERS spectra of R6G with Au@ Ag NPs.

100 random locations of SERS assays were performed on 10^{-4} M of R6G to examine the SERS reproducibility of Au@Ag NPs. The mapping image was also shown (Fig. 4e), with a uniform color distribution, demonstrating that the enhancement effect is consistent and highly reproducible. Fig. 4f shows the SERS spectra of R6G with Au@Ag NPs.

3.2 SERS spectra of creatinine and urea nitrogen

In order to detect Scr and BUN qualitatively and quantitatively, SERS spectra of creatinine and urea nitrogen were acquired in standard solutions and in fetal bovine serum solutions, respectively. Characteristic peaks of creatinine at 574 cm^{-1}, 613 cm^{-1}, 681 cm^{-1}, 847 cm^{-1}, 922 cm^{-1}, 1424 cm^{-1}, and 1758 cm^{-1} were clearly observed in both standard solutions and fetal bovine serum solutions (Fig. 5a and c).A characteristic peak at 1001 cm^{-1} was present in all urea nitrogen solutions (Fig. 5b and d). We got the same characteristic peaks between standard solutions and serums, which means two biomarkers can be detected in the serum. The peak positions and their attributions are shown in Table 2. All the main Raman characteristic peaks obtained from the experiments correspond with those in previous reports of creatinine and urea nitrogen.[50,51] For both biomarkers, the peaks were well matched in both types of solutions, yet both biomarkers presented slightly lower signal intensity and SNR in fetal bovine serum solutions. It was due to the complex environment of serum samples and this has been very common in SERS research. In this work, we chose the 681 cm^{-1} peak to represent creatinine and the 1001 cm^{-1} peak to represent urea nitrogen for further quantification, both of which were obvious and consistent peaks.

3.3 SERS detection for single and mixed biomarker solutions

We have made single biomarker solution assays and mixed biomarker solution assays for a series of concentrations of Scr and BUN, respectively (Fig. 6a and c). SERS spectra of Scr were acquired for concentrations ranging from 10^{-1} to 10^{-6} M (0.0113 mg dl^{-1} to 1131.2 mg dl^{-1}). SERS spectra of BUN were acquired for concentrations ranging from 50 to 0.28 mg dl^{-1}. The range of measurement is orders of magnitude wider than the possible content in the human body, showing excellent sensitivity and adequate testing range. The limit of detection (LOD) is the lowest concentration of analyte that can be calculated in the background signal according to the IUPAC:[52,53]

$$C_{LOD} = 3\delta_{bi}S \quad (4)$$

where δ_{bi} is the standard deviation of the blank signal, measured multiple times, and $S = \Delta\text{concentration}/\Delta\text{intensity}$ at a certain characteristic peak.

The LODs of Scr and BUN were calculated to be 2.08 × 10^{-7} mol L^{-1} and 0.11 mg dl^{-1}, respectively. The linearity between the concentrations and the SERS intensities at 681 cm^{-1} and 1001 cm^{-1} peaks were ideal with correlation coefficients $R^2 = 0.9789$ and 0.9842, respectively (Fig. 6b and d).

Compared with characteristic peaks of single solutions, Scr and BUN had the same peaks (Fig. 6e and f), showing that two biomarkers can be measured simultaneously with SERS.

To demonstrate the ability of the proposed method in the diagnosis of renal function based on two biomarkers, 16 groups of mixed BUN and Scr serum solutions at different concentrations were measured with SERS. The concentrations are shown in Table 1. The spectra of the 16 groups are shown in Fig. 7, and each spectrum was an average of 10 measurements. For better

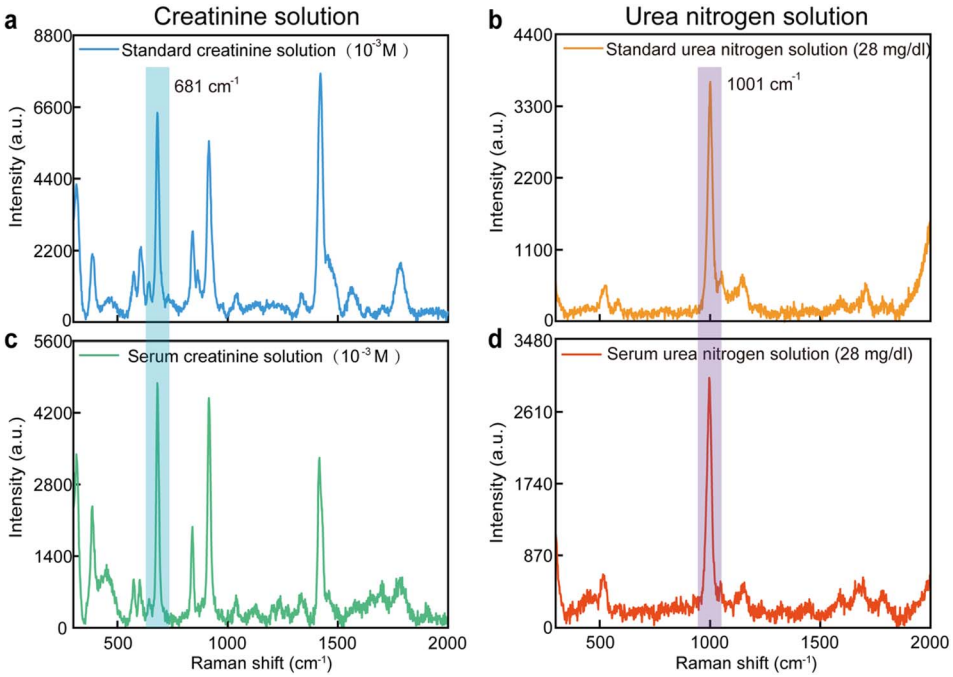

Fig. 5 SERS spectra of creatinine and urea nitrogen in standard and fetal bovine serum solutions. (a) SERS spectra of creatinine (10^{-3} M) in standard solution. (b) SERS spectra of urea nitrogen (28 mg dl^{-1}) in standard solution. (c) SERS spectra of creatinine (10^{-3} M) in fetal bovine serum solution. (d) SERS spectra of urea nitrogen (28 mg dl^{-1}) in serum solution.

Table 2 Band assignment for creatinine and urea nitrogen

	SERS peaks in refs. [50] and 51	Au@Ag NP enhanced SERS (cm^{-1})	Assignment
Creatinine	576	574	C–H bending
	602	613	C–H bending
	678	681	N–H bending
	833	847	N–H bending
	900	922	C–H rocking or C–C bending
	1426	1424	C–H bending
	1708	1758	C–O stretching
Urea nitrogen	548	516	C–N vibrations
	1010	1001	N–C–N stretches

visualization, 4 groups with a constant BUN concentration and varying Scr concentrations were shown in one graph. In each graph, the constant biomarker presented stable signal intensity, while the varying concentrations resulted in a gradient of intensity. However, in the mixed solutions, there were subtle differences in similar concentrations to differentiate. Therefore, conventional methods suffer during quantification of mixed solutions.

3.4 Prediction of the biomarker concentration based on CNN

The 640 experimentally collected SERS spectra were randomly split into 80% for training and 20% for testing.[54] The CNN model was optimized to reach an accurate prediction. An error back-propagation algorithm along with the stochastic gradient descent optimization method, adaptive moment estimation (Adam) was used to iteratively optimize the CNN parameters to minimize the loss function.[55] After iterating for 5000 epochs, the loss function continued to decrease and finally stabilized close to 0. The CNN model showed great performance in concentration regression, and the training results of BUN and Scr are shown in Fig. 8a and b.

The 1D-CNN model was trained using Python (v3.8.8) and TensorFlow (v2.3.1, Google Inc). The operation time required for testing one SERS spectrum was less than 0.1 ms when performed by using a computer configured with NVIDIA Titan RTX (GPU) and Intel Xeon Platinum 8160 (CPU), indicating that the assessment can achieve real-time effective kidney function prediction by using the proposed CNN model.

We also compared the regression performance of 1D-CNN, FNN and other conventional regression methods such as SVR and PLSR (Table 3). The R^2 (training R_t^2 and testing R_p^2) were

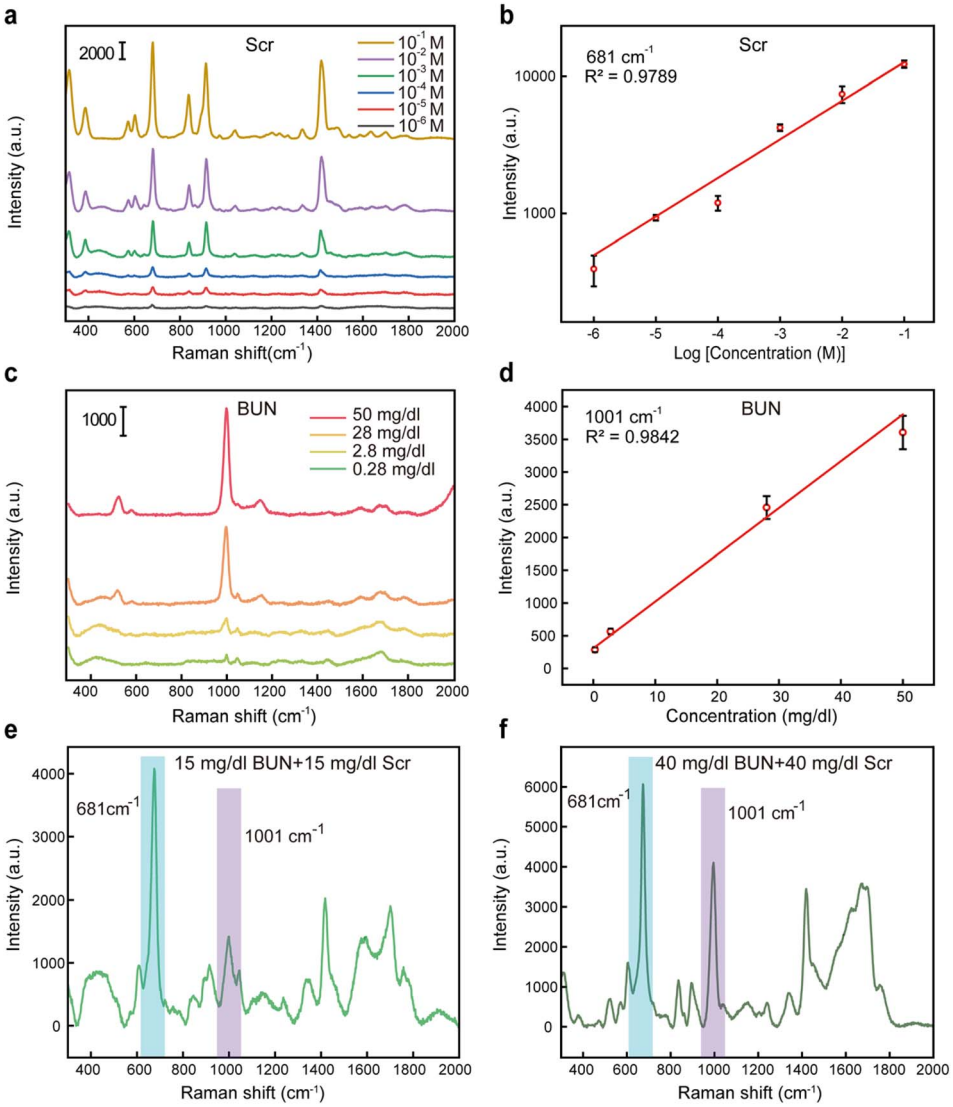

Fig. 6 SERS spectra of two substances and their mixture in fetal bovine serum. (a) and (c) SERS spectra of creatinine and urea nitrogen at a series of concentrations using Au@Ag NPs in fetal bovine serum, respectively. (b) The linear relationship between the Scr concentration and SERS intensity at 681 cm^{-1}. (d) The linear relationship between the BUN concentration and SERS intensity at 1001 cm^{-1}. (e) and (f) SERS spectra of Scr and BUN mixed at a concentration of 1 : 1 (15 mg dl^{-1}) and 1 : 1 (40 mg dl^{-1}), respectively.

used to evaluate the performance of each model. The R_t^2 obtained from all four models approached 0.9976, 0.9689, 0.9715, and 0.9832, respectively. However, there were some differences in testing results of R_p^2 among all four models for prediction. The 1D-CNN model showed the best prediction performance, reaching the highest value of R_p^2 0.9871, shown in Fig. 8a and b. FNN ranked second with an R_p^2 of 0.9684. The performance of SVR and PLSR was not so satisfactory because of the inadequate capacity to extract features and because it lacks learning abilities. The conventional regression methods SVR and PLSR achieved poorer results for R_p^2 values of 0.9332 and 0.9470.

By comparison, the deep learning model 1D-CNN achieved better results than other models in quantitative analysis of SERS spectra with subtle differences. In addition, RMSEs of Scr and BUN were calculated by using CNN in the test set to be 0.27 mg dl^{-1} and 1.45 mg dl^{-1}, respectively, representing accurate predictions. This is because CNN has powerful learning ability during the training process, mimicking the way the human brain operates. Each kernel and neuron in the model were trained during the error back-propagation algorithm, automatically extracting features from the input spectrum. In contrast, features in machine learning models are specially selected and defined. The proposed 1D-CNN model provided an effective approach for the prediction and recognition of the SERS dataset.

The proposed system was convenient and accurate in quantifying renal biomarkers in serum and could be further improved in several aspects. For example, a more advanced SERS substrate array could be employed, such as metal nanoparticles immobilized on a solid substrate[56,57] and nanostructures fabricated on a solid substrate by nanolithography,[58,59] improving the sensitivity and robustness

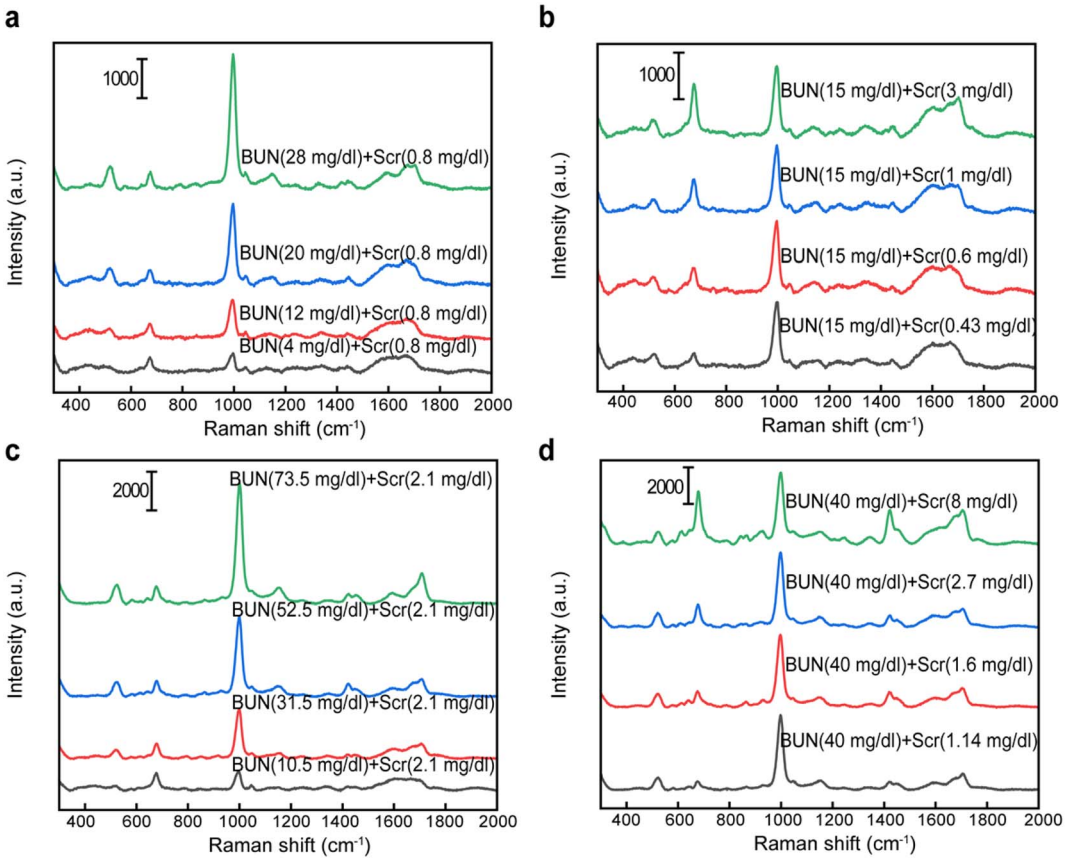

Fig. 7 (a)–(d) SERS spectra of 16 groups of mixed solutions (BUN and Scr) separated into 4 graphs.

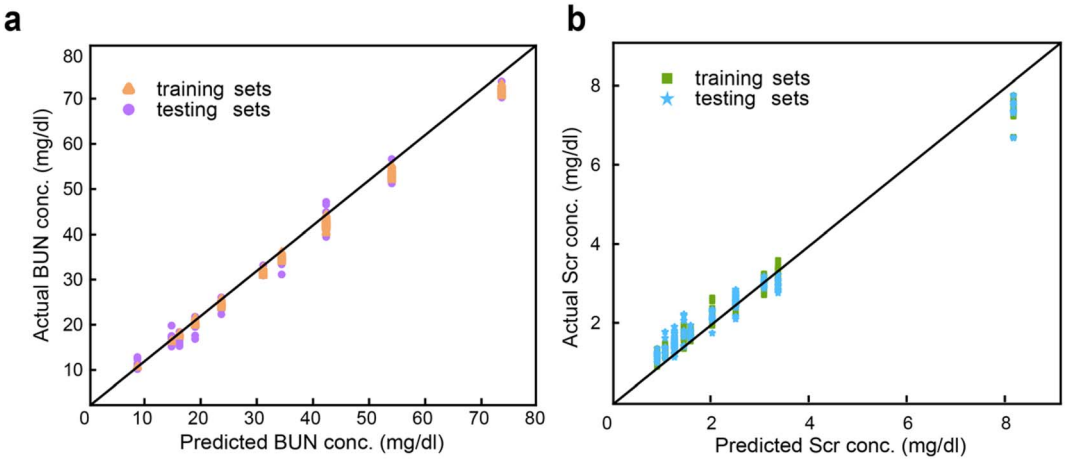

Fig. 8 Performance of the CNN-based kidney healthy prediction system. Plots of predicted concentrations *vs.* actual concentrations of training and testing sets of BUN (a) and Scr (b).

Table 3 Predictive results obtained by all of the four models

Model	1-CNN	SVR	PLS	FNN
R_t^2	0.9976	0.9689	0.9715	0.9832
R_P^2	0.9871	0.9332	0.9470	0.9684

of SERS detection. In addition, the number of 16 groups of SERS datasets in this study was still limited, and the precision of the diagnosed kidney health level can be more detailed with expansion of training numbers and concentration levels of biomarkers. Moreover, the SERS signal may be directly analyzed by using an all-optical diffractive neural network integrated on CMOS,[60,61] processing the incident Raman information at the

speed of light. In the future, we anticipate that the deep learning-enhanced SERS detection approach will greatly accelerate the development of kidney health assessment and a wide variety of clinical diagnostic applications.

4. Conclusions

In this work, we proposed an effective kidney health assessment system that can simultaneously detect and quantify two renal biomarkers, creatinine and urea nitrogen, in a serum environment. An Au@Ag nanoparticle substrate was developed to perform highly sensitive SERS detection and a CNN model was utilized to process the complicated spectra of mixed solutions. The renal assessment system exhibited the advantages of excellent predictive performance (0.9871 R^2) and fast speed (<0.1 ms/detection). It is believed that the deep learning-enhanced SERS detection approach can lead to a giant leap for clinical diagnosis and for quick identification of potential patients for early treatment.

Conflicts of interest

There are no conflicts to declare.

Acknowledgements

This work was supported by the National Key Research and Development Program of China (2017YFC0110200 and 2021YFB2802300) and National Natural Science Foundation of China (61805143).

References

1 R. Bellomo, J. A. Kellum and C. Ronco, *Lancet*, 2012, **380**, 756–766.
2 S. Narayanan and H. D. Appleton, *Clin. Chem.*, 1980, **26**, 1119–1126.
3 S. Uchino, *Curr. Opin. Crit. Care.*, 2010, **16**, 562–567.
4 M. S. Parmar, *Br. Med. J.*, 2002, **325**, 85–90.
5 T. D. Bjornsson, *Clin. Pharmacokinet.*, 1979, **4**, 200–222.
6 J. L. Lyman, *Emerg. Med. Clin. N. Am.*, 1986, **4**, 223–233.
7 S. I. Gunnarsson, R. Palsson, G. Sigurdsson and O. S. Indridason, *Nephron Clin. Pract.*, 2013, **123**, 22–27.
8 K. Kashani, M. H. Rosner and M. Ostermann, *Eur. J. Intern. Med.*, 2020, **72**, 9–14.
9 C. Leordean, V. Canpean and S. Astilean, *Spectrosc. Lett.*, 2020, **45**, 550–555.
10 I. W. Mahdiasanti, A. Sabarudin and H. Sulistyarti, *IOP Conf. Ser.: Mater. Sci. Eng.*, 2019, 546.
11 A. Kamal, *Indian J. Fundam. Appl. Life Sci.*, 2014, **4**, 199–202.
12 J. R. Delanghe and M. M. Speeckaert, *Nephrol. Dial. Transplant. Plus*, 2011, **4**, 83–86.
13 W. Junge, B. Wilke, A. Halabi and G. Klein, *Clin. Chim. Acta*, 2004, **344**, 137–148.
14 M. H. Kroll, N. A. Roach, B. Poe and R. J. Elin, *Clin. Chem.*, 1987, **33**, 1129–1132.
15 S. Zhou, R. Zuo, Z. Zhu, D. Wu, K. Vasa, Y. Deng and Y. Zuo, *Anal. Methods*, 2013, **5**, 1307–1311.
16 Y. Yang and C. Lin, *Biomicrofluidics*, 2015, **9**, 022402.
17 B. Lindbäck and A. Bergman, *Clin. Chem.*, 1989, **35**, 835–837.
18 L. Han, X. Huang, L. Zhang, Q. Zhang, J. Wang, H. Lin, J. Yan, J. Zhuang and X. Huang, *J. Pharm. Biomed.*, 2019, **162**, 124–129.
19 M. Yildirimel, M. N. Atalar, S. Abusoglu, D. E. Onmaz, A. Sivrikaya, G. Abusoglu and A. Unlu, *Turkish J. Biochem.*, 2021, **46**, 263–271.
20 S. Schlücker, *Angew. Chem., Int. Ed.*, 2014, **53**, 4756–4795.
21 B. Sharma, R. R. Frontiera, A. Henry, E. Ringe and R. V. Duyne, *Mater. Today*, 2012, **15**, 16–25.
22 S. Laing, K. Gracie and K. Faulds, *Chem. Soc. Rev.*, 2016, **45**, 1901–1918.
23 H. Kearns, R. Goodacre, L. E. Jamieson, D. Graham and K. Faulds, *Anal. Chem.*, 2017, **89**, 12666–12673.
24 Q. Ding, J. Wang, X. Chen, H. Liu, Q. Li, Y. Wang and S. Yang, *Nano Lett.*, 2020, **20**, 7304–7312.
25 N. Cheng, D. Chen, B. Lou, J. Fu and H. Wang, *Biosens. Bioelectron.*, 2021, **186**, 113–246.
26 X. Yan, S. Zhang, H. Fu and H. Qu, *Spectrochim. Acta, Part A*, 2020, **226**, 117589.
27 C. Ni, D. Wang and Y. Tao, *Spectrochim. Acta, Part A*, 2019, **209**, 32–39.
28 Y. Lecun, Y. Bengio, and G. Hinton, *The Handbook of Brain Theory and Neural Networks*, 1995, p. 3361.
29 S. Pande, J. Chowdhury and T. Pal, *J. Phys. Chem. C*, 2011, **115**, 10497–10509.
30 L. Song, K. Mao, X. Zhou and J. Hu, *Talanta*, 2016, **146**, 285–290.
31 B. Aswathy, G. Sony and K. G. Gopchandran, *Plasmonics*, 2014, **9**, 1323–1331.
32 M. D. Welch and R. D. Mullins, *Annu. Rev. Cell Dev. Biol.*, 2002, **18**, 247–288.
33 N. Chen, Y. Yuan, P. Lu, L. Wang, X. Zhang, H. Chen and P. Ma, *Biomed. Opt. Express*, 2021, **12**, 7673–7688.
34 C. Persaud, U. Sandesara, V. Hoang, J. Tate, W. Latack and D. Dado, *Case Reports in Nephrology*, 2021, 2021.
35 K. D. Liu, J. Himmelfarb, E. Paganini, T. A. Ikizler, S. H. Soroko, R. L. Mehta and G. M. Chertow, *Clin. J. Am. Soc. Nephrol*, 2006, **1**, 915–919.
36 J. Antonio, A. Ellerbroek, T. Silver, L. Vargas, A. Tamayo, R. Buehn and C. A. Peacock, *Nutr. Metab.*, 2016, **2016**, 9104792.
37 R. Corsetti, A. Barassi, S. Perego, V. Sansoni, A. Rossi, C. A. L. Damele, G. M. D'eril, G. Banfi and G. Lombardi, *Amino Acids*, 2016, **48**, 183–192.
38 J. Kang, G. Fulop and A. H. Friedman, *Acta Ophthalmol.*, 1998, **66**, 407–412.
39 S. M. Zia Ziabari, S. Rimaz, A. Shafaghi, M. Shakiba, Z. Pourkazemi, E. Karimzadeh and M. Amoukhteh, *Arch. Acad. Emerg. Med.*, 2019, **7**, 30.
40 D. B. Morgan, M. E. Carver and R. B. Payne, *Br. Med. J.*, 1977, **2**, 929–932.

41 M. C. Huang, M. E. Chen, H. C. Hung, H. C. Chen, W. T. Chang, C. H. Lee, Y. Y. Wu, H. C. Chiang and S. J. Hwang, *J. Ren. Nutr.*, 2008, **18**, 187–194.
42 K. Bhatia, P. Misra, A. Singh, B. Mukherjee and V. N. Ambade, *Int. J. Biomed.*, 2019, **3**, 6–180.
43 J. B. Dossetor, *Ann. Intern. Med.*, 1966, **65**, 1287–1299.
44 W. R. Clark, B. A. Mueller, M. A. Kraus and W. L. Macias, *Kidney Int.*, 1998, **54**, 554–560.
45 L. Zhang, Q. Li, W. Tao, B. Yu and Y. Du, *Anal. Bioanal. Chem.*, 2010, **398**(4), 1827–1832.
46 L. Li and W. S. Chin, *Food Chem.*, 2021, **357**, 129717.
47 N. Cheng, D. Chen, B. Lou, J. Fu and H. Wang, *Biosens. Bioelectron.*, 2021, **186**, 113246.
48 Y. S. Chen, H. L. Jiang, C. Y. Lin, X. P. Jia and P. Ghamisi, *IEEE Trans. Geosci. Remote Sens.*, 2016, **54**, 6232–6251.
49 Y. Zhou, G. Zhao, J. Bian, X. Tian, X. Cheng, H. Wang and H. Chen, *ACS Appl. Mater. Interfaces*, 2020, **12**, 28532–28538.
50 K. Karn-Orachai and A. Ngamaroonchote, *Appl. Surf. Sci.*, 2021, **546**, 149092.
51 M. Verma, T. K. Naqvi, S. K. Tripathi, M. M. Kulkarni and P. K. Dwivedi, *Environ. Technol. Innov.*, 2021, **24**, 102033.
52 P. Ma, L. Wang, L. Xu, J. Li, X. Zhang and H. Chen, *Eur. Food Res. Technol.*, 2020, **246**, 239–251.
53 H. Fang, X. Zhang, S. J. Zhang, L. Liu, Y. M. Zhao and H. J. Xu, *Sens. Actuators, B*, 2015, **213**, 452–456.
54 A. Gholamy, V. Kreinovich and O. Kosheleva, *Int. J. Intell. Technol. Appl. Stat.*, 2018, **11**, 105–111.
55 H. Bai and S. H. G. Chan, arXiv, 2020, preprint, **2012**, 15685.
56 W. J. Cho, Y. Kim and J. K. Kim, *ACS Nano*, 2012, **6**, 249–255.
57 S. Dong, Y. Wang, Z. Liu, W. Zhang, K. Yi, X. Zhang, X. Zhang, C. Jiang, S. Yang, F. Wang and X. Xiao, *ACS Appl. Mater. Interfaces*, 2020, **12**, 5136–5146.
58 Z. Jin, W. Sun, Y. Ke, C. Shih, G. Paulus, Q. H. Wang, B. Mu, P. Yin and M. S. Strano, *Nat. Commun.*, 2013, **4**, 1–9.
59 N. B. Kiremitler, S. Pekdemir, J. Patarroyo, S. Karabel, I. Torun, V. F. Puntes and M. S. Onses, *ACS Macro Lett.*, 2017, **6**, 603–608.
60 E. Goi, X. Chen, Q. Zhang, B. P. Cumming, S. Schoenhardt, H. Luan and M. Gu, *Light: Sci. Appl.*, 2021, **10**, 1–11.
61 X. Lin, Y. Rivenson, N. T. Yardimci, M. Veli, Y. Luo, M. Jarrahi and A. Ozcan, *Science*, 2018, **361**, 1004–1008.

